THE JOURNAL OF PHYSICAL CHEMISTRY B

pubs.acs.org/JPCB Article

Conformational Entropy from Restricted Bond-Vector Motion in Proteins: The Symmetry of the Local Restrictions and Relation to NMR Relaxation

Netanel Mendelman and Eva Meirovitch*

Cite This: J. Phys. Chem. B 2020, 124, 4284−4292

Read Online

ACCESS | Metrics & More | Article Recommendations

ABSTRACT: Locally mobile bond-vectors contribute to the conformational entropy of the protein, given by $S_k \equiv S/k = -\int(P_{eq} \ln P_{eq})d\Omega - \ln\int d\Omega$. The quantity $P_{eq} = \exp(-u)/Z$ is the orientational probability density, where Z is the partition function and u is the spatially restricting potential exerted by the immediate internal protein surroundings at the site of the motion of the bond-vector. It is appropriate to expand the potential, u, which restricts local rotational reorientation, in the basis set of the real combinations of the Wigner rotation matrix elements, D^L_{0K}. For small molecules *dissolved in* anisotropic media, one typically keeps the lowest even L, $L = 2$, *nonpolar* potential in axial or rhombic form. For bond-vectors *anchored at* the protein, the lowest odd L, $L = 1$, *polar* potential is to be used in axial or rhombic form. *Here, we investigate the effect of the symmetry and polarity of these potentials on* S_k. For $L = 1$ ($L = 2$), S_k is the same (differs) for parallel and perpendicular ordering. The plots of S_k as a function of the coefficients of the rhombic $L = 1$ ($L = 2$) potential exhibit high-symmetry (specific low-symmetry) patterns with parameter-range-dependent sensitivity. Similar statements apply to analogous plots of the potential minima. S_k is also examined as a function of the order parameters defined in terms of u. Graphs displaying these correlations, and applications illustrating their usage, are provided. The features delineated above are generally useful for devising orienting potentials that best suit given physical circumstances. They are particularly useful for bond-vectors acting as NMR relaxation probes in proteins, when their restricted local motion is analyzed with stochastic models featuring Wigner-function-made potentials. The relaxation probes could also be molecules adsorbed at surfaces, inserted into membranes, or interlocked within metal−organic frameworks.

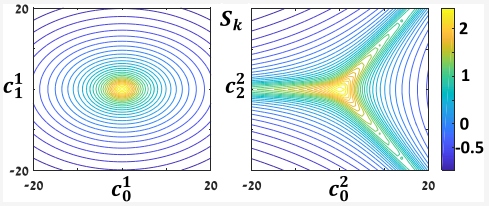

1. INTRODUCTION

Typically, proteins exhibit internal mobility. Within their scope, various structural moieties, notably bond-vectors, move locally in the presence of spatial restrictions exerted by the immediate (internal) protein surroundings. These restrictions result from the anisotropic nature of the local structure. In their presence, the bond-vector orientation is distributed nonuniformly even in cases where the local motion is undetectable, while the local ordering can be measured. The pertinent probability density functions yield conformational entropy, S_k, defined (in units of the Boltzmann constant, k) as $S_k = -\int(P_{eq} \ln P_{eq})d\Omega - \ln\int d\Omega$.[1] $P_{eq} = \exp(-u)/Z$ is the normalized probability density, where Z is the partition function and u is the restricting local potential. The quantity of interest is *the change* in conformational entropy, ΔS_k, between two protein states, entailed by a physical process.[1−3] Usually, the second term in the expression for S_k cancels out in calculating ΔS_k.

In some cases, the restricted local bond-vector motion is observable (following appropriate isotope labeling) with NMR relaxation. Stochastic models for NMR relaxation analysis feature explicit potentials,[4,5,7,8] which straightforwardly yield S_k (refs 6, 10). While this study refers to bond-vectors in proteins in general, it connects with NMR relaxation through the subset of NMR-active bond-vectors.[11,12] Let us examine this connection.

The traditional method for the analysis of NMR relaxation in proteins is model-free (MF).[13] In the MF formalism, the local spatial restrictions are expressed in terms of the squared generalized order parameter, S^2, rather than a potential function. Analytical expressions connecting S^2 with S_k for very simple axial potentials were developed;[1,12] an empirical relation which does so for several simple axial potentials was also devised.[1] A dictionary for protein side-chain entropies derived from S^2 was established in ref 14. In that study, empirical relations connecting S^2 with S_k were developed utilizing reference configurational entropies and order parameters determined with molecular dynamics (MD) simulations. Actual cases using this method appear in the

Received: March 26, 2020
Revised: April 22, 2020
Published: May 1, 2020

literature.[15] In the context of ligand binding, Wand et al. devised the empirical relation called "model-independent entropy meter" that features adjustable coefficients, which project the experimentally measured methyl-related changes in motion across the entire protein and ligand.[12]

Thus, within the scope of the MF conceptualizations, the S^2-to-S_k conversion features in some cases simple axial potentials.

In recent years, we developed the two-body coupled-rotator slowly relaxing local structure (SRLS) approach[16−18] for the analysis of NMR relaxation in proteins.[19−22] In SRLS, the local potential is expanded in the basis set of the real linear combinations of the Wigner rotation matrix elements, D^L_{0K} (in brief, real Wigner functions).[16,19] In accordance with typical experimental data, the lowest even L terms, and in some cases the lowest odd L terms, have been kept, yielding $u = -c^2_0 D^2_{00} - c^2_2 (D^2_{02} + D^2_{0-2})$ for nonpolar ordering[17,18,20−22] and $u = -c^1_0 D^1_{00} - c^1_1 (D^1_{0-1} - D^1_{01})$ for polar ordering.[23−26]

Nonpolar ($L = 2$) ordering prevails when there is inversion symmetry with respect to the origin of the director (preferred probe orientation) frame as for rigid molecules *dissolved* in anisotropic media.[4,5] Polar ($L = 1$) ordering prevails when there is no inversion symmetry with respect to the origin of the director frame. This is the case for bond-vectors *anchored* at the protein[23,24] (or any other relaxation probe anchored at the entity that represents the local director). In view of the various approximations, admixtures are most appropriate. The fact that MF, and in many cases SRLS, have treated local ordering from the nonpolar ($L = 2$) perspective is due to the fact that the theories for proteins originate in theories for small molecules.

In principle, the two-term potentials depicted above can be enhanced in SRLS by adding terms to its expression. In practice, this is often hindered by limited experimental data. We pursued the idea of potential enhancement outside of the scope of SRLS[25,26] as follows. Linear combinations of real Wigner functions with $L = 1-4$ were created and optimized against the corresponding potential of mean force (POMF) obtained with MD simulations. Comparison between the best-fit Wigner function and the POMF indicated that the set of terms with $L = 1-4$ suffices for obtaining good agreement. Moreover, using such optimized potentials, new insights into the dimerization of the Rho GTPase binding domain of plexin-B1 (in brief, plexin-B1 RBD) were gained.[26] In future work, we plan to incorporate these potentials *unchanged* into SRLS data-fitting schemes. This will improve the picture of structural dynamics to be obtained due to better potentials, and better characterization of this picture as additional parameters can now be determined with data fitting.

The POMFs are themselves restricting potentials that can yield conformational entropy. However, they are statistical functions and as such cannot be utilized in the development promoted in this study, which is based on explicit potentials.

Thus, we have at hand explicit axial and rhombic, polar and nonpolar, fairly accurate Wigner-function-made local potentials. This constitutes a rich source for conformational entropy derivation. To optimize this process in terms of the suitability of the local potential and the accuracy of the pertinent conformational entropy, it is important to determine the relation between potential form, symmetry, parity, etc. and conformational entropy. We do this here for the $L = 1$ and 2 potentials depicted above. Correlation graphs are provided, and their utilization is illustrated with several applications. NMR relaxation analysis using SRLS directly can benefit from this study.

A theoretical summary is given in Section 2. Our results and their discussion are described in Section 3, and our conclusions appear in Section 4.

2. THEORETICAL BACKGROUND

2.1. Restricting Potentials. The orienting potential, $U(\Omega)$, associated with restricted rotational reorientation, is typically given by the expansion in Wigner rotation matrix elements, $D^L_{0K}(\Omega)$[4,5]

$$u(\Omega) \equiv U(\Omega)/kT = \sum_{\infty}^{L=1} \sum_{+L}^{M=-L} \sum_{+L}^{K=-L} c^L_{MK} D^L_{MK}(\Omega) \tag{1}$$

where the Euler angles, Ω, describe the orientation of the probe relative to the director, which is the direction of preferential orientation in the restricting surroundings.[4,5] Note that u and the coefficients featured by eq 1 are dimensionless.

It is usually assumed that the director is uniaxial (see ref 17 for the introduction of biaxiality in a manner involving one additional variable angle). Consequently, the "quantum number" M in eq 1 is zero and $\Omega = (0, \theta, \varphi)$. One has to ensure that the potential is real; this is achieved by expanding $u(\Omega)$ in the basis set of the real combinations of the Wigner rotation matrix elements (the real Wigner functions). Finally, the infinite expansion in eq 1 has to be truncated. Keeping only the lowest even L terms, one has[5]

$$u(\theta, \varphi) - c^2_0 D^2_{00}(\theta, \varphi) - c^2_2 [D^2_{02}(\theta, \varphi) + D^2_{0-2}(\theta, \varphi)] \tag{2}$$

For $c^2_0 > 0$, the main ordering axis orients preferentially parallel to the director; this is termed parallel ordering. For $c^2_0 < 0$, the main ordering axis orients preferentially perpendicular to the director; this is termed perpendicular ordering.[4,5] Keeping only the lowest odd L terms, one has:[23,24]

$$u(\theta, \varphi) = -c^1_0 D^1_{00}(\theta, \varphi) - c^1_1 [D^1_{0-1}(\theta, \varphi) - D^1_{01}(\theta, \varphi)] \tag{3}$$

For $c^1_0 > 0$ ($c^1_0 < 0$), the primary polar axis is parallel to the $+z$ ($-z$) axis of the local ordering frame. For $c^1_1 > 0$ ($c^1_1 < 0$), the primary polar axis is tilted in the $+zx$ ($-zx$) plane of the local ordering frame.[4,23]

Exploring the relationship between these (and further enhanced) potentials and the conformational entropy, S_k, is very broad in scope. The connection with SRLS,[19−22] which applies to proteins in solution, has been delineated above. The SRLS limit where the protein motion is frozen is the microscopic-order-macroscopic-disorder (MOMD) approach,[27] which we developed for proteins in the solid state.[28−32] SRLS and MOMD were originally developed for electron spin resonance (ESR) applications in complex fluids and proteins.[16−18,27] In all of these theoretical approaches, the local potential is expressed in terms of real Wigner functions. The present study is relevant to all of them and, in general, to any established stochastic model for spin relaxation analysis.[4,5]

2.2. Parameters of Interest Defined in Terms of the Restricting Potentials. *2.2.1. Order Parameters.* Order parameters are ensemble averages of real Wigner functions defined in terms of restricting potentials. Here, we are using the order parameters[4,23]

$$S^L_0 = \langle D^L_{00}(0, \theta, 0) \rangle, \quad L = 1, 2 \tag{4a}$$

$$S^1_1 = \langle D^1_{0-1}(\theta, \varphi) - D^1_{01}(\theta, \varphi) \rangle \tag{4b}$$

https://dx.doi.org/10.1021/acs.jpcb.0c02662
J. Phys. Chem. B 2020, 124, 4284−4292

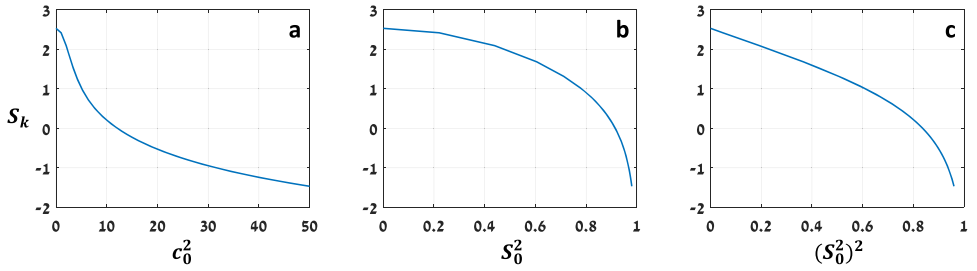

Figure 1. Conformational entropy, S_k, as a function of (a) the coefficient, c_0^2, of the potential $u = -c_0^2 D_{00}^2$, (b) the order parameter, $S_0^2 = \langle D_{00}^2 \rangle$, and (c) the squared order parameter, $(S_0^2)^2$. c_0^2 ranges from 0 to 50; S_0^2 and $(S_0^2)^2$ range from 0 to 1.

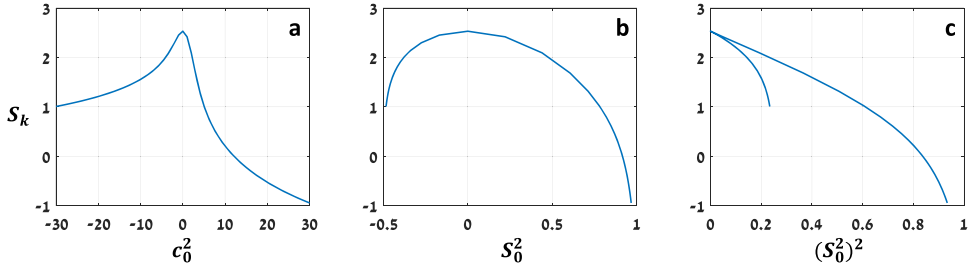

Figure 2. Conformational entropy, S_k, as a function of (a) the coefficient, c_0^2, of the potential $u = -c_0^2 D_{00}^2$, (b) the order parameter, $S_0^2 = \langle D_{00}^2 \rangle$, and (c) the squared order parameter, $(S_0^2)^2$. c_0^2 ranges from −20 to 20, S_0^2 ranges from −0.5 to 1.0, and $(S_0^2)^2$ ranges from 0 to 1. The long branch in Figure 2c is associated with $c_0^2 > 0$ and $S_0^2 > 0$; the short branch is associated with $c_0^2 < 0$ and $S_0^2 < 0$.

$$S_2^2 = \langle D_{02}^2(\theta, \varphi) + D_{0-2}^2(\theta, \varphi) \rangle \tag{4c}$$

The normalized probability density function required to calculate these ensemble averages is given by

$$\frac{\int D_{0K}^L(0, \theta, \varphi)\, e^{-u(\theta,\varphi)} \sin\theta \, d\theta d\varphi}{\int e^{-u(\theta,\varphi)} \sin\theta \, d\theta d\varphi} \tag{5}$$

where $u(\theta,\varphi)$ is the restricting potential.

2.2.2. Conformational Entropy. The entropy divided by k, S_k, is defined as[1]

$$S_k = -\int (P_{eq} \ln P_{eq}) d\Omega - \ln \int d\Omega \tag{6}$$

where $P_{eq} = \exp(-u)/Z$ is the normalized probability density, Z is the partition function, and u is the restricting potential. The change in conformational entropy is given by[1]

$$\Delta S_k = \Delta\left[-\int (P_{eq} \ln P_{eq}) d\Omega\right] \tag{7}$$

In this study, u is given by eqs 2 or 3 and ΔS_k is calculated using eqs 6 and 7. The coefficients c_0^2, c_2^2, c_0^1, and c_1^1 may be positive or negative.

Let us relate to the model-free treatment of eq 7. The local spatial restrictions are implicit in the squared generalized order parameter, S^2, defined as[13]

$$S^2 = \sum_{K=0,\pm1,\pm2} |\langle D_{0K}^2 \rangle \langle D_{0-K}^2 \rangle| \tag{8}$$

where $\langle \cdots \rangle$ denotes ensemble average. The functions in eq 8 are the (complex) Wigner rotation matrix elements with $L = 2$ and $K = -L,...,L$. We have shown that[10]

$$S^2 = (S_0^2)^2 + 0.5\,(S_2^2)^2 \tag{9}$$

For wobble-in-a-cone and one-dimensional (1D) harmonic oscillator, analytical expressions connecting S^2 with S_k were developed.[1,12] For several simple axial potentials, the following empirical expression was developed[1]

$$S_k = A + \ln \pi[3 - (1 + 8S)^{1/2}] \tag{10}$$

The parameter A is adjusted to suit the individual potentials. This equation was obtained with a different parameterization in ref 14. Only positive values of S (which, as pointed out above, correspond to parallel ordering) are considered. Empirical relations for methyl groups were developed within the scope of a dictionary-type framework in ref 14 (see above). A comprehensive empirical relation was developed in ref 12 (see above).

3. RESULTS AND DISCUSSION

3.1. Axial Potentials. The first axial ($K = 0$) even L term in the Wigner function expansion yields the potential $u = -c_0^2 D_{00}^2 = -c_0^2\,(1.5\cos^2\theta - 0.5)$. Figure 1a–c shows S_k as a function of the coefficient $c_0^2 > 0$, the order parameter $S_0^2 = \langle D_{00}^2 \rangle$, and the squared order parameter $(S_0^2)^2$, respectively. A comparison with MF may be conducted given that both S and S_0^2 range from 0 to 1. Note that $S_0^2 = 0$ corresponds to $c_0^2 = 0$ and $S_0^2 = 1$ corresponds to $c_0^2 \to \infty$. We use $0 \le c_0^2 \le 50$; any number greater than approximately 20 is virtually infinity.

Figure 1c shows S_k as a function of $(S_0^2)^2$. The conformational entropy, S_k, was calculated according to eq 6; S_0^2 was calculated in terms of the potential $u = -c_0^2 D_{00}^2$ according to eq 4a. Figure 1 of ref 1 shows S_k as a function of S^2 obtained using eq 10 for several simple potentials. All of the curves in Figure 1 of ref 1 agree qualitatively with the curve in Figure 1c; none agrees with it quantitatively, although many of the simple potentials considered in ref 1 are limiting cases of $u = -c_0^2 D_{00}^2$.

As expected, in all three panels of Figure 1, the entropy decreases with increasing potential or ordering strength. In the region of interest for proteins, where $1 \lesssim c_0^2 \lesssim 10$, the S_k versus c_0^2 curve is substantially steeper, hence more sensitive, than the other two curves.

https://dx.doi.org/10.1021/acs.jpcb.0c02662
J. Phys. Chem. B 2020, 124, 4284−4292

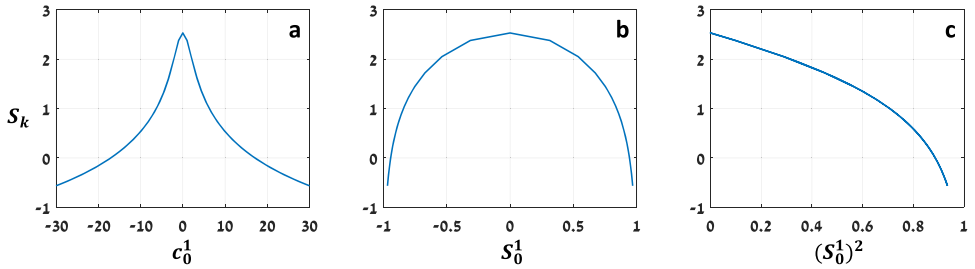

Figure 3. Conformational entropy, S_k, as a function of (a) the coefficient, c_0^1, of the potential $u = -c_0^1 D_{00}^1$, (b) the order parameter, $S_0^1 = \langle D_{00}^1 \rangle$, and (c) the squared order parameter, $(S_0^1)^2$. c_0^1 ranges from −30 to 30, S_0^1 from −1.0 to 1.0, and $(S_0^2)^2$ from 0 to 1.

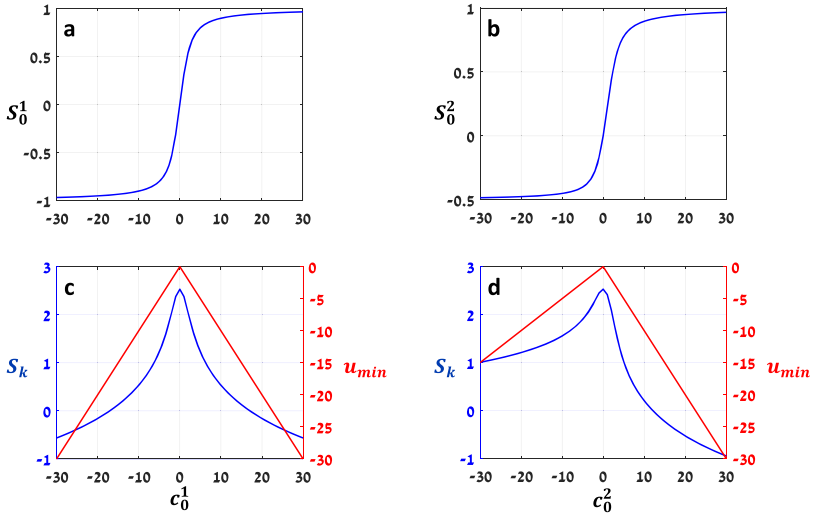

Figure 4. Order parameter, S_0^1, as a function of the coefficient, c_0^1, of the potential $u = -c_0^1 D_{00}^1$ (a). Order parameter, S_0^2, as a function of the potential coefficient, c_0^2, of the potential $u = -c_0^2 D_{00}^2$ (b). Conformational entropy, S_k (blue), and the minimum, u_{min}, of $u = -c_0^1 D_{00}^1$ (red), as a function of c_0^1 (c). Conformational entropy, S_k (blue), and the minimum, u_{min}, of $u = -c_0^2 D_{00}^2$ (red), as a function of c_0^2 (d).

Let us focus on c_0^2. As indicated, nonpolar ($L = 2$) local ordering may be parallel or perpendicular. We[19−22] and others[33−35] found that typically the main ordering axis at N−H sites in proteins is $C^\alpha - C^\alpha$. Recalling that the director is given by the equilibrium orientation of the N−H bond, it may be deduced that, within a good approximation, perpendicular ordering prevails at these sites.[20−22] In general, the sign of the coefficient, c_0^2, in eq 2, *obtained with data fitting*, determines whether the local ordering is parallel or perpendicular. This information enters the expression for S_k straightforwardly (eq 6). When MF is used, data fitting determines S^2. For perpendicular ordering to enter S_k, one has to use $-S$ in expressions such as eq 10. This has not been done, with implications illustrated below.

Figure 2a−c is analogous to Figure 1a−c, except that now both parallel and perpendicular orderings are featured by considering the full parameter range of c_0^2. For parallel ordering, one has $0 \le c_0^2 < \infty$ and $0 < S_0^2 < 1$; for perpendicular ordering, one has $0 > c_0^2 > -\infty$ and $0 \ge S_0^2 \ge -0.5$. The S_k patterns for $c_0^2 < 0$ and $c_0^2 > 0$ differ; so do the S_k patterns for $S_0^2 < 0$ and $S_0^2 > 0$. Figure 2c shows S_k as a function of $(S_0^2)^2$. A second branch yielded by negative S_0^2 values is featured in the 0−1 range; this branch is missing in MF.

Let us focus on the simplest axial polar case. $L = 1$ potentials are treated in refs 23, 26. In ref 24, we analyzed the ^{15}N−H relaxation data from the third immunoglobulin binding domain of streptococcal protein G (GB3) with rhombic $L = 1$ or 2 potentials and found that the results differ. Importantly, we found that the process by which GB3 binds to its cognate Fab fragment has polar character.[24] Thus, potential parity is both influential and important.

Figure 3 refers to the potential $u = -c_0^1 D_{00}^1 = -c_0^1 \cos\theta$. Figure 3a shows S_k as a function of c_0^1 for $-30 \le c_0^1 \le 30$, Figure 3b shows S_k as a function of S_0^1 for $-1 \le S_0^1 \le 1$, and Figure 3c shows S_k as a function of $(S_0^1)^2$. In Figure 3a,b S_k is the same for positive and negative c_0^1 (S_0^1), i.e., for the primary polar axis pointing along $+z$ and $-z$.[23] A single branch is featured by $(S_0^1)^2$ (Figure 3c).

We extend the analysis by including in it order parameters and the minima of the $L = 1$ and 2 potentials. Figure 4a shows $S_0^1 = \langle D_{00}^1 \rangle$ as a function of c_0^1 for $-30 \le c_0^1 \le 30$, and Figure 4b shows $S_0^2 = \langle D_{00}^2 \rangle$ as a function of c_0^2 for $-30 \le c_0^2 \le 30$. For $L = 1$, S_0^1 is the same for $+c_0^1$ (primary polar axis pointing along $+z$) and $-c_0^1$ (primary polar axis pointing along $-z$); for $L = 2$, S_0^2 is not the same for $+c_0^2$ (parallel ordering) and $-c_0^2$ (perpendicular ordering).

Figure 4c shows S_k as a function of c_0^1 (blue), superposed on the minimum of the $u = -c_0^1 \cos\theta$ potential, denoted u_{min}, as a function of c_0^1 (red). The corresponding scales are depicted on the left and right ordinates. As one would expect, primary polar axes pointing along $+z$ or $-z$ yield the same patterns.

Figure 4d shows S_k as a function of c_0^2 (blue), superposed on u_{min} of $u = -c_0^2$ $(1.5 \cos\theta^2 - 0.5)$ as a function of c_0^2 (red). The corresponding scales are depicted on the left and right ordinates. Both patterns differ for parallel ($c_0^2 > 0$) and perpendicular ($c_0^2 < 0$) ordering. In particular, if the potential

https://dx.doi.org/10.1021/acs.jpcb.0c02662
J. Phys. Chem. B 2020, 124, 4284−4292

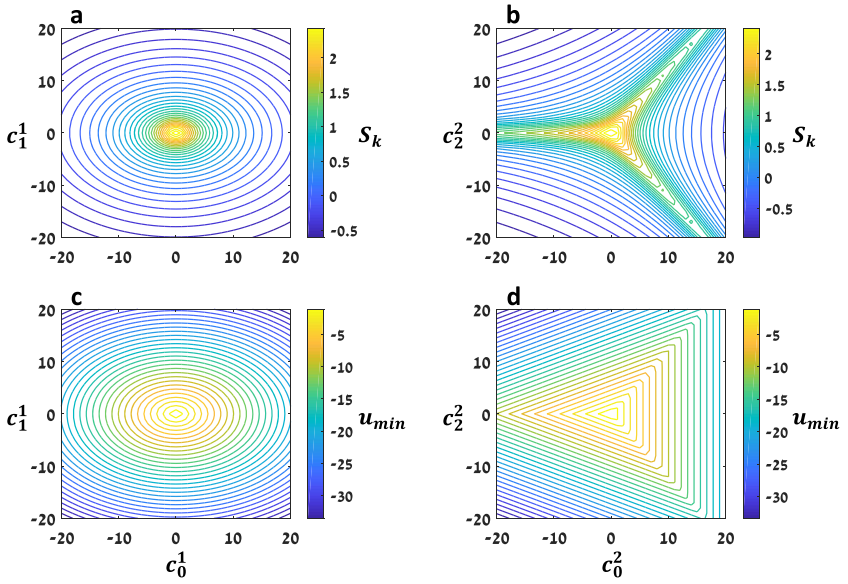

Figure 5. Conformational entropy, S_k, as a function of the coefficients, c_0^1 and c_1^1, of the potential $u = -c_0^1 D_{00}^1 - c_1^1 (D_{0\text{-}1}^1 - D_{01}^1)$ (a). Conformational entropy, S_k, as a function of the coefficients, c_0^2 and c_2^2, of the potential $u = -c_0^2 D_{00}^2 - c_2^2 (D_{02}^2 + D_{0\text{-}2}^2)$ (b). The minimum, u_{min}, of $u = -c_0^1 D_{00}^1 - c_1^1 (D_{0\text{-}1}^1 - D_{01}^1)$ as a function of c_0^1 and c_1^1 (c). The minimum, u_{min}, of $u = -c_0^2 D_{00}^2 - c_2^2 (D_{02}^2 + D_{0\text{-}2}^2)$ as a function of c_0^2 and c_2^2 (d). Color codes are on the right of each panel. A total of 1681 data points were used in generating each panel of this figure.

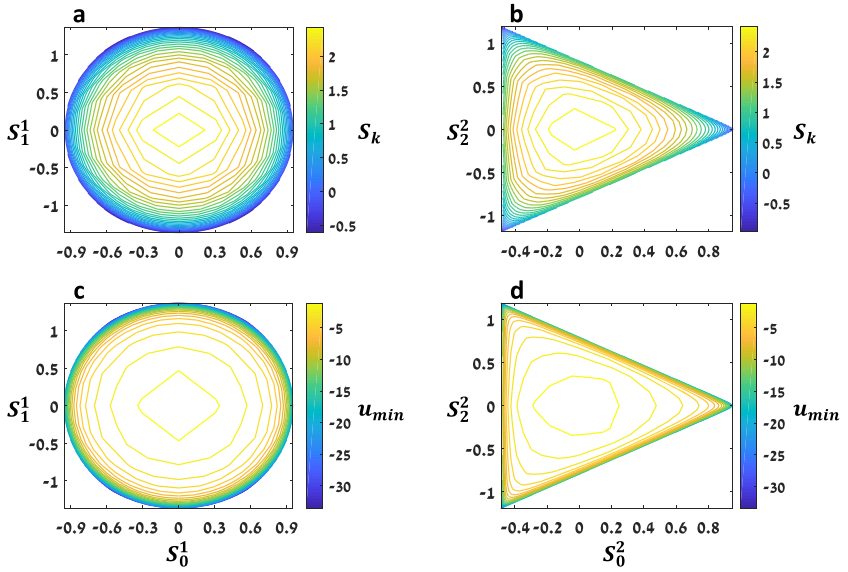

Figure 6. Conformational entropy, S_k, as a function of the order parameters, S_0^1 and S_1^1, defined in terms of the potential $u = -c_0^1 D_{00}^1 - c_1^1 (D_{0\text{-}1}^1 - D_{01}^1)$ (a). Conformational entropy, S_k, as a function of the order parameters, S_0^2 and S_2^2, defined in terms of the potential $u = -c_0^2 D_{00}^2 - c_2^2 (D_{02}^2 + D_{0\text{-}2}^2)$ (b). u_{min} of $u = -c_0^1 D_{00}^1 - c_1^1 (D_{0\text{-}1}^1 - D_{01}^1)$ as a function of S_0^1 and S_1^1 (c). u_{min} of $u = -c_0^2 D_{00}^2 - c_2^2 (D_{02}^2 + D_{0\text{-}2}^2)$ as a function of S_0^2 and S_2^2 (d). Color codes and number of data points as in Figure 5.

minimum is $-a$ (at $\theta = 0°$) for parallel ordering, it will be $-a/2$ (at $\theta = 90°$) for perpendicular ordering.

3.2. Rhombic Potentials. Equations 2 and 3 show the functional forms of the rhombic $L = 2$ and 1 potentials, respectively. Figure 5a,b shows S_k as a function of the potential coefficients c_0^1 and c_1^1 (c_0^2 and c_2^2). Figure 5c,d shows u_{min} as a function of the coefficients c_0^1 and c_1^1 (c_0^2 and c_2^2). In all of the Figure 5 simulations, and in the simulations of Figures 6 and 7, 1681 data points were used; the same results were obtained with a larger number of data points.

The curves depicted in Figure 5a represent the group of points with coordinates (c_0^1, c_1^1) that yield the same conformational entropy, S_k; those depicted in Figure 5b represent the group of points with coordinates (c_0^2, c_2^2) that yield the same conformational entropy. We call these curves S_k isolines. Figure 5c,d shows the u_{min} isolines for the $L = 1$ and 2 potentials, respectively. The color codes for the values of S_k and u_{min} are given on the right of each figure. In Figure 5a,b, intense orange corresponds to large entropy and intense blue corresponds to small entropy. In Figure 5c,d, intense orange corresponds to shallow potentials and intense blue corresponds to deep potentials.

$L = 1$ potentials (Figure 5a,c), which are shallow and nearly axial (small $|c_0^1|$ and $|c_1^1|$), yield large entropy; those which are deep and highly rhombic (large $|c_0^1|$ and $|c_1^1|$) yield small entropy. In-between the changes are less monotonic for S_k

https://dx.doi.org/10.1021/acs.jpcb.0c02662
J. Phys. Chem. B 2020, 124, 4284−4292

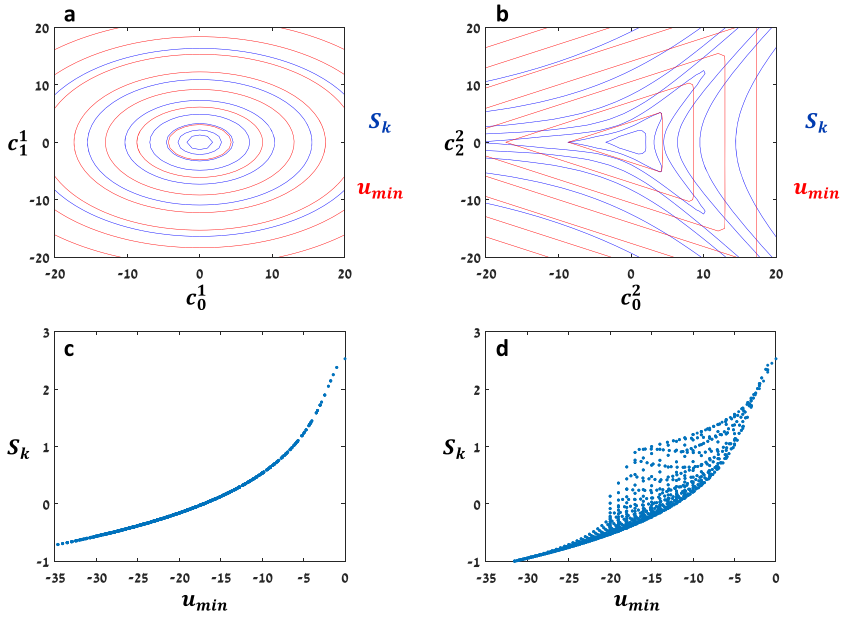

Figure 7. (a) Superposed conformational entropy, S_k (blue), and potential minimum, u_{min} (red), as a function of the coefficients, c_0^1 and c_1^1, of the potential $u = -c_0^1 D_{00}^1 - c_1^1 (D_{0\text{-}1}^1 - D_{01}^1)$. (b) S_k of (a) as a function of u_{min} of (a). (c) Superposed conformational entropy, S_k (blue), and potential minimum, u_{min} (red), as a function of the coefficients, c_0^2 and c_2^2, of the potential $u = -c_0^2 D_{00}^2 - c_2^2 (D_{02}^2 + D_{0\text{-}2}^2)$. (d) S_k of (c) as a function of u_{min} of (c). Number of data points as in Figure 5.

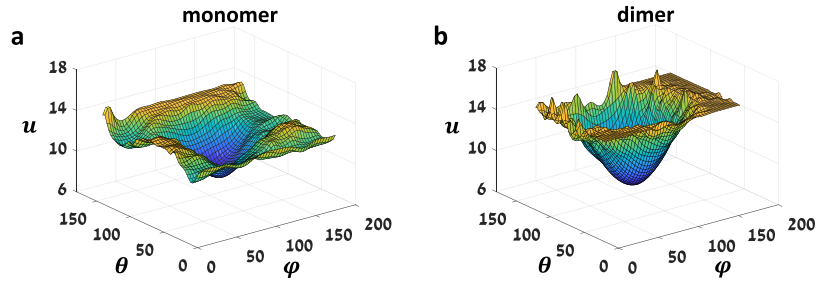

Figure 8. MD-derived potentials of mean force for the N−H bonds of residue G73 of plexin-B1 RBD in monomer (Figure 8a) and dimer (Figure 8b) forms.[9,36,37] The minima of these potentials (in units of kT) are 8.4 and 7.8, respectively.

(Figure 5a) and more monotonic for u_{min} (Figure 5c). The S_k patterns are more sensitive in the middle, and the u_{min} patterns are more sensitive in the outer region. The situation is more complicated for $L = 2$, which is associated with asymmetric shapes of the S_k and u_{min} isoline patterns (Figure 5b,d). While $+c_2^2$ and $-c_2^2$ yield the same isoline patterns, $+c_0^2$ and $-c_0^2$ yield different isoline patterns. The S_k patterns are more sensitive in the middle, and the u_{min} patterns are more sensitive in the outer region, in a distinctive manner. Note that the high sensitivity of the S_k isoline patterns ensures good certainty in S_k.

Figure 6a−d is analogous to Figure 5a−d, with the coordinates being order parameters instead of potential coefficients. (S_0^1, S_1^1) are defined in terms of (c_0^1, c_1^1), and (S_0^2, S_2^2) are defined in terms of (c_0^2, c_2^2) (cf. Equations 2, 3 and 4a−c). The isolines of Figure 6 are much more dispersed in conformation space than the isolines of Figure 5. Good certainty in S_k is expected for potentials of relatively great, and intermediate, strength, and relatively great, and intermediate, rhombicity, as the S_k isolines vary most in these regions.

N−H bonds in well-structured regions of the protein conformation feature relatively strong and highly rhombic potentials.[20,21] In this case, it is preferable to use the correlation graphs of Figure 6. C−CH_3 bonds in proteins feature relatively weak potentials.[20,21] In that case, it is preferable to use the correlation graphs of Figure 5 (see examples below).

Figure 7a shows superposed S_k and u_{min} isolines as a function of the coefficients c_0^1 and c_1^1 of the $L = 1$ potential. The objective is to examine the correlation between S_k and u_{min}. One can recognize a one-to-one correspondence; its precise form is revealed by Figure 7c, where S_k is depicted as a function of u_{min}. Figure 7b shows superposed S_k and u_{min} isolines as a function of the coefficients c_0^2 and c_2^2 of the $L = 2$ potential. The relation between S_k and u_{min} is intricate. Indeed, Figure 7d shows that, in general, multiple S_k values correspond to a given value of u_{min}.

The utilization of the correlation graphs of Figures 1−6 is illustrated below.

3.3. Applications. *3.3.1. Example 1.* Statistical potentials of mean force (POMFs) can be derived directly from MD trajectories.[25,26,36,37] Figure 8a,b shows images of two POMFs representing two protein states before and after a physical event. They belong to residue G73 of plexin-B1 RBD in monomer and dimer forms,[26] but we consider them representative of a general situation where the only information available consists of POMFs.

https://dx.doi.org/10.1021/acs.jpcb.0c02662
J. Phys. Chem. B 2020, 124, 4284−4292

The estimated minima are (in units of kT) 8.4 and 7.8. One could use eq 7 to determine ΔS_k. However, at this stage, it is not known whether the local ordering is parallel or perpendicular. Taking $u = -c_0^2 D_{00}^2$ as a reasonable approximation, and using *conjointly* the graphs of Figure 2a–c, it might be possible to distinguish between these two situations. Figure 2c is likely to be particularly useful in this context. With this information in hand, one could proceed effectively with detailed analysis, where rhombic symmetry is allowed for.

3.3.2. Example 2. ^{15}N relaxation of the major urinary protein I (MUP-I) and its complex with the pheromone 2-sec-butyl-4,5-dihydrothiazol were studied with MF at 300 K in early work.[38] The authors of ref 38 found that pheromone binding brings about *increase* in conformational entropy. We studied this system with SRLS in the 283–308 K range using $u = -c_0^2 D_{00}^2$ and assuming parallel ordering, to find that below approximately 300 K, S_k indeed increases, but above that temperature, it decreases, upon pheromone binding.[9]

At 308 K, c_0^2 is on the order of 15–17 in both forms of MUP-I. At 283 K, the majority of the c_0^2 values are on the order of 25 in the free form and between 15 and 20 in the bound form (Figure 7 of ref 9). ΔS_k is small at both temperatures. The S_k versus positive c_0^2 curve in Figure 2a shows that the dependence of S_k on c_0^2 is nearly linear for large c_0^2 and much steeper for smaller c_0^2. Therefore decreasing the pressure at 283 K would lower c_0^2 differentially increasing Δc_0^2, hence ΔS_k. Thereby, the change in conformational entropy upon pheromone binding will be determined with enhanced certainty in the interesting temperature range.

3.3.3. Example 3. Table 1 shows the average values of the potential coefficients $\langle c_0^2 \rangle$ and $\langle c_2^2 \rangle$ for all of the methyl moieties of the complex of Ca^{2+}–calmodulin with the peptide smMLCKp at the temperatures depicted (rows 1 and 2). It also shows $\langle c_0^2 \rangle$ and $\langle c_2^2 \rangle$ of the alanine and methionine methyl groups at 295 K (rows 3 and 4).[39]

Table 1. Average Potential Coefficients, $\langle c_0^2 \rangle$ and $\langle c_2^2 \rangle$, of All of the Methyl Groups of the Complex of Ca^{2+}–Calmodulin with the Peptide smMLCLp at 288 and 308 K (Rows 1 and 2), and $\langle c_0^2 \rangle$ and $\langle c_2^2 \rangle$ of Alanine (A) and Methionine (M) at 295 K (Rows 3 and 4)[a]

	T, K	$\langle c_0^2 \rangle$	$\langle c_2^2 \rangle$	S_k
1	288	0.92	−0.68	1.69
2	308	0.39	−0.74	1.77
3	295	0.22	−0.98	1.72
4	295	0.65	−0.50	1.76

[a]Reproduced with permission from ref 39. Copyright 2011 of the American Chemical Society.

The coefficients $\langle c_0^2 \rangle$ and $\langle c_2^2 \rangle$ in Table 1 represent rhombic $L = 2$ potentials. SRLS calculations where the potentials have rhombic symmetry are considerably more time-consuming than SRLS calculations, where the potentials have axial symmetry. One can permute the axes of the local ordering frame so that, in the new frame, the symmetry of the potential is different.[5,40] The permuted coefficients, $\hat{c}_0^2$ and $\hat{c}_2^2$, are given by[40]

$$\hat{c}_0^2 = -c_0^2/2 - \sqrt{\frac{3}{2}}\, c_2^2 \tag{11a}$$

$$\hat{c}_2^2 = \left(\sqrt{\frac{3}{2}}\, c_0^2 - c_2^2\right)/2 \tag{11b}$$

The following situation is envisioned for the methyl groups of a given protein designated for SRLS analysis. One selects representative methyl moieties and determines c_0^2 and c_2^2 with SRLS data fitting. Using Figure 5b, the corresponding isolines are identified. For small c_0^2 and small c_2^2, typical of methyl moieties in proteins,[39] every S_k isoline has two points with $c_2^2 \approx 0$. In some cases, c_0^2 of such points will be similar to the $\hat{c}_0^2$ data of the representative residues. For residues with data similar to those of the representative residues (appropriate criteria will have to be specified), it will be useful to use in SRLS calculations $\hat{c}_0^2$ and $\hat{c}_2^2 \approx 0$. The geometric information will have to be updated accordingly.

3.3.4. Example 4. Table 2 shows S_0^2 and S_2^2 obtained with SRLS analysis of the N–H bonds of residues Q2 and A26 of the third immunoglobulin binding domain of streptococcal protein G (GB3) using the rhombic $L = 2$ potential.[41]

Table 2. S_0^2 and S_2^2 of Residues Q2 and A26 of GB3 Obtained with SRLS Analysis of ^{15}N Relaxation.[41] S_k Derived from the c_0^2 and c_2^2 Values That Yielded These S_0^2 and S_2^2 Values (eqs 2, 4a, and 4c)[a]

1	2	3	4	5
residue	structural element	S_0^2	S_2^2	S_k
Q2	β_1 strand	−0.49	1.08	−0.37
A26	α helix	−0.42	1.13	−0.70

[a]Reproduced with permission from ref 41. Copyright 2012 of the American Chemical Society.

The points (S_0^2, S_2^2) with values (−0.49, 1.08) and (−0.42, 1.13) are located in the upper left corner of Figure 6b, as they represent strong perpendicular ordering and large rhombicity. Figure 6b refers to the rhombic $L = 2$ potential, whereas Figure 6a refers to the rhombic $L = 1$ potential. Figure 6a shows better sensitivity in the region under consideration than Figure 6b. This indicates that analyzing ^{15}N relaxation in compact proteins such as GB3 using the rhombic $L = 1$ potentials is likely to yield local potentials, hence pertinent order parameters and conformational entropy, which are determined with enhanced certainty. This is useful information for future work.

3.3.5. Future Prospects. It is of interest to compare for a given NMR relaxation probe dynamic structures associated with the same value of S_k. This can be accomplished by the following strategy:[1] Analyze NMR relaxation data of a given probe with SRLS and determine the "experimental" c_0^2 and c_2^2 values;[2] calculate S_k (eq 6) and use Figure 5b to determine the corresponding isoline;[3] select representative pairs of c_0^2 and c_2^2 belonging to this isoline;[4] use these c_0^2 and c_2^2 pairs *unchanged* in SRLS data fitting and determine the corresponding local motional rates and local geometry;[5] and compare the results of steps 1 and 4.

3.3.6. Comments. (1) Lately, pressure-dependent[42] and temperature-dependent[43] studies have been performed in the context of conformational entropy derivation. The results of such studies might be useful in a project where explicit SRLS potentials and statistical MD-derived POMFs improve one another within the scope of an iterative scheme. We contemplate devising such a scheme in future work. (2) We derive conformational entropy from restricted local motions. In

https://dx.doi.org/10.1021/acs.jpcb.0c02662
J. Phys. Chem. B 2020, 124, 4284–4292

the context of NMR relaxation, the pertinent restrictions are "observed" sources.[2] There exists a different approach pursued, e.g., in ref 44, where the entropy changes are derived using an "entropy meter". The latter is an expression comprising S^2 from observed sources as well as adjustable coefficients that "project the experimentally measured changes in motion across the entire protein and ligand". The projected changes are "unobserved" sources. Such contributions are outside the scope of our study.

4. CONCLUSIONS

The local potentials, u, at the site of mobile bond-vectors in proteins have been expressed in terms of the real linear combinations of the Wigner rotation matrix elements, D^L_{0K} (in brief, real Wigner functions), with $L = 1$ or 2. From them, the conformational entropy, S_k, has been derived. To determine the effect of the symmetry (axial or rhombic) and L-parity of the local potential on the associated conformational entropy, correlation graphs between S_k and the coefficients of u, as well as between S_k and the order parameters defined in terms of u, have been created. The S_k patterns obtained are highly specific and exhibit distinctive parameter-range-dependent sensitivity. This lays the groundwork for devising potentials for the determination of S_k that best suit given physical circumstances.

NMR relaxation analysis has been invoked as a physical method that can profit substantially from these results. So can any physical method where the local restrictions are expressed in terms of real Wigner functions.

We use here the amide bond and the methyl moiety of proteins as examples of NMR relaxation probes. Additional examples are molecular moieties adsorbed as surfaces, embedded in membranes, or interlocked in metal−organic frameworks.

AUTHOR INFORMATION

Corresponding Author

Eva Meirovitch − *The Mina and Everard Goodman Faculty of Life Sciences, Bar-Ilan University, Ramat-Gan 52900, Israel;* orcid.org/0000-0001-5117-5079; Phone: 972-3-531-8049; Email: eva.meirovitch@biu.ac.il

Author

Netanel Mendelman − *The Mina and Everard Goodman Faculty of Life Sciences, Bar-Ilan University, Ramat-Gan 52900, Israel*

Complete contact information is available at: https://pubs.acs.org/10.1021/acs.jpcb.0c02662

Notes

The authors declare no competing financial interest.

ACKNOWLEDGMENTS

The authors acknowledge support from the Israel Science Foundation (grant 369/15 to E.M.) and the Binational Israel−United States Science Foundation (grant 2016097 to E.M. and Jack H. Freed).

REFERENCES

(1) Yang, D.; Kay, L. E. Contributions to Conformational Entropy Arising from Bond Vector Fluctuations Measured from NMR-Derived Order Parameter: Application to Protein Folding. *J. Mol. Biol.* **1996**, *263*, 369−382.

(2) Akke, M.; Brüschweiler, R.; Palmer, A. G., III NMR Order Parameters and Free Energy: an Analytical Approach and its Application to Cooperative Ca^{2+} Binding by Calbindin D_{9k}. *J. Am. Chem. Soc.* **1993**, *115*, 9832−9833.

(3) Li, Z.; Raychaudhuri, S.; Wand, A. J. Insights into the Local Residual Entropy of Proteins Provided by NMR Relaxation. *Protein Sci.* **1996**, *5*, 2647−2650.

(4) *The Molecular Dynamics of Liquid Crystals*; Luckhurst, G. R.; Veracini, C. A., Eds.; Kluwer Academic Publishers: The Netherlands, 1994.

(5) Polnaszek, C. F.; Freed, J. H. Electron Spin Resonance Studies of Anisotropic Ordering, Spin Relaxation and Slow Tumbling in Liquid Crystalline Solvents. *J. Phys. Chem. A* **1975**, *79*, 2283−2306.

(6) Massi, F.; Palmer, A. G., III Temperature Dependence of NMR Order Parameters and Protein Dynamics. *J. Am. Chem. Soc.* **2003**, *125*, 11158−1159.

(7) Tchaicheeyan, O.; Meirovitch, E. An SRLS Study of ^{2}H Methyl-Moiety Relaxation and Related Conformational Entropy in Free and Peptide-Bound PLC$_\gamma$1C SH2. *J. Phys. Chem. B* **2016**, *120*, 10695−10705.

(8) Tchaicheeyan, O.; Meirovitch, E. Conformational Entropy from NMR Relaxation in Proteins: the SRLS Perspective. *J. Phys. Chem. B* **2017**, *121*, 758−768.

(9) Žídek, L.; Meirovitch, E. Conformational Entropy from Slowly Relaxing Local Structure Analysis of ^{15}N−H Relaxation in Proteins: Application to Pheromone Binding to MUP-I in the 283−308 K Temperature Range. *J. Phys. Chem. B* **2017**, *121*, 8684−8692.

(10) Zerbetto, M.; Meirovitch, E. ^{15}N−H-Related Conformational Entropy Changes Entailed by Plexin-B1 RBD Dimerization: A Combined Molecular Dynamics/NMR Relaxation Approach. *J. Phys. Chem. B* **2017**, *121*, 3007−3015.

(11) Stone, M. J. NMR Relaxation Studies of the Role of Conformational Entropy in Protein Stability and Ligand Binding. *Acc. Chem. Res.* **2001**, *34*, 379−388.

(12) Wand, A. J.; Sharp, K. A. Measuring Entropy in Molecular Recognition by Proteins. *Annu. Rev. Biophys.* **2018**, *47*, 41−61.

(13) Lipari, G.; Szabo, A. Model-Free Approach to the Interpretation of Nuclear Magnetic Resonance Relaxation in Macromolecules. 1. Theory and Range of Validity. *J. Am. Chem. Soc.* **1982**, *104*, 4546−4559.

(14) Li, D.-W.; Brüschweiler, R. A Dictionary for Protein Side-Chain Entropies from NMR Order Parameters. *J. Am. Chem. Soc.* **2009**, *131*, 7226−7227.

(15) Solomentsev, G.; Diehl, C.; Akke, M. Conformational Entropy of FK506 Binding of FBP12 Determined by Nuclear Magnetic Resonance Relaxation and Molecular Dynamics Simulations. *Biochemistry* **2018**, *57*, 1451−1461.

(16) Polimeno, A.; Freed, J. H. A Many-Body Stochastic Approach to Rotational Motions in Liquids. *Adv. Chem. Phys.* **1993**, *83*, 89−204.

(17) Polimeno, A.; Freed, J. H. Slow-Motional ESR in Complex Fluids: The Slowly Relaxing Local Structure Model of Solvent Cage Effects. *J. Phys. Chem. B* **1995**, *99*, 10995−11006.

(18) Liang, Z.; Freed, J. H. An Assessment of the Applicability of Multifrequency ESR to Study the Complex Dynamics of Biomolecules. *J. Phys. Chem. B* **1999**, *103*, 6384−6396.

(19) Tugarinov, V.; Liang, Z.; Shapiro, Y. E.; Freed, J. H.; Meirovitch, E. A Structural Mode-Coupling Approach to ^{15}N NMR Relaxation in Proteins. *J. Am. Chem. Soc.* **2001**, *123*, 3055−3063.

(20) Meirovitch, E.; Shapiro, Y. E.; Polimeno, A.; Freed, J. H. Protein Dynamics from NMR: the SRLS Analysis Compared with MF Analysis. *J. Phys. Chem. A* **2006**, *110*, 8366−8396.

(21) Meirovitch, E.; Shapiro, Y. E.; Polimeno, A.; Freed, J. H. Structural Dynamics of Biomolecules by NMR: The Slowly Relaxing Local Structure Approach. *Prog. Nucl. Magn. Reson. Spectrosc.* **2010**, *56*, 360−405.

(22) Zerbetto, M.; Polimeno, A.; Meirovitch, E. General Theoretical/Computational Tool for Interpreting NMR Spin Relaxation in Proteins. *J. Phys. Chem. B* **2009**, *113*, 13613−13625.

(23) Tchaicheeyan, O.; Freed, J. H.; Meirovitch, E. Local Ordering at Mobile Sites in Proteins from Nuclear Magnetic Resonance Relaxation: The Role of Site Symmetry. *J. Phys. Chem. B* **2016**, *120*, 2886−2898.
(24) Tchaicheeyan, O.; Meirovitch, E. Polar Versus Non-Polar Local Ordering at Mobile Sites in Proteins: Slowly Relaxing Local Structure Analysis of ^{15}N Relaxation in the Third Immunoglobulin-Binding Domain of Streptococcal Protein G. *J. Phys. Chem. B* **2016**, *120*, 386−395.
(25) Tchaicheeyan, O.; Mendelman, N.; Zerbetto, M.; Meirovitch, E. Local Ordering at Mobile Sites in Proteins: Combining Perspectives from NMR Relaxation and Molecular Dynamics. *J. Phys. Chem. B* **2019**, *123*, 2745−2755.
(26) Mendelman, N.; Zerbetto, M.; Buck, M.; Meirovitch, E. Local Ordering at the N−H Sited of the Rho GTPase Binding Domain of Plexin-B1: Impact of Dimerization. *J. Phys. Chem. B* **2019**, *123*, 8019−8033.
(27) Meirovitch, E.; Nayeem, A.; Freed, J. H. Analysis of Protein-Lipid Interactions Based on Model Simulations of ESR Spectra. *J. Phys. Chem. C* **1984**, *88*, 3454−3465.
(28) Meirovitch, E.; Liang, Z.; Freed, J. H. Protein Dynamics in the Solid State from ^{2}H NMR Line Shape Analysis: A Consistent Perspective. *J. Phys. Chem. B* **2015**, *119*, 2857−2868.
(29) Meirovitch, E.; Liang, Z.; Freed, J. H. Protein Dynamics in the Solid State from ^{2}H NMR Lineshape Analysis. II MOMD Applied to C−D and C−CD_3 Probes. *J. Phys. Chem. B* **2015**, *119*, 14022−14032.
(30) Meirovitch, E.; Liang, Z.; Freed, J. H. MOMD Analysis of NMR Lineshapes from Aβ-Amyloid Fibrils: A New Tool for Characterizing Molecular Environments in Protein Aggregates. *J. Phys. Chem. B* **2018**, *122*, 4793−4801.
(31) Meirovitch, E.; Liang, Z.; Freed, J. H. Phenyl-Ring Dynamics in Amyloid Fibrils and Proteins: The Microscopic-Order-Macroscopic-Disorder Perspective. *J. Phys. Chem. B* **2018**, *122*, 8675−8684.
(32) Meirovitch, E.; Liang, Z.; Freed, J. H. Protein Dynamics in the Solid State from ^{2}H NMR Line Shape Analysis. III. MOMD in the Presence of Magic Angle Spinning. *Solid State Nucl. Magn. Reson.* **2018**, *89*, 35−44.
(33) Lienin, S. F.; Bremi, T.; Brütscher, B.; Brüschweiler, R.; Ernst, R. R. Anisotropic Intramolecular Backbone Dynamics of Ubiquitin Characterized by NMR Relaxation and MD Computer Simulation. *J. Am. Chem. Soc.* **1998**, *120*, 9870−9879.
(34) Fadel, A. R.; Jin, D. Q.; Montelione, G. T.; Levy, R. M. Crankshaft Motions of the Polypeptide Backbone in Molecular Dynamics Simulations of Human Type-Alpha Transforming Growth-Factor. *J. Biomol. NMR* **1995**, *6*, 221−226.
(35) Bremi, T.; Brüschweiler, R. Locally Anisotropic Internal Polypeptide Backbone Dynamics by NMR Relaxation. *J. Am. Chem. Soc.* **1997**, *119*, 6672−6673.
(36) Zerbetto, M.; Buck, M.; Meirovitch, E.; Polimeno, A. Integrated Computational Approach to the Analysis of NMR Relaxation in Proteins: Application to Main Chain ^{15}N−^{1}H and Global Dynamics of Rho GTPase Binding Domain of Plexin-B1. *J. Phys. Chem. B* **2011**, *115*, 376−388.
(37) Zerbetto, M.; Anderson, R.; Bouquet-Bonnet, S.; Rech, M.; Zhang, L.; Meirovitch, E.; Polimeno, A.; Buck, M. Analysis of ^{15}N-^{1}H NMR Relaxation in Proteins by a Combined Experimental and Molecular Dynamics Simulation Approach: Picosecond-Nanosecond Dynamics of the Rho GTPase Binding Domain of Plexin-B1 in the Dimeric State Indicates Allosteric Pathways. *J. Phys. Chem. B* **2013**, *117*, 174−184.
(38) Zídek, L.; Novotny, M. V.; Stone, M. J. Increased Protein Backbone Conformational Entropy upon Hydrophobic Ligand Binding. *Nat. Struct. Biol.* **1999**, *6*, 1118−1121.
(39) Shapiro, Y. E.; Polimeno, A.; Freed, J. H.; Meirovitch, E. Methyl Dynamics of a Ca^{2+}-Calmodulin-Peptide Complex from NMR/SRLS. *J. Phys. Chem. B* **2011**, *115*, 354−365.
(40) Barnes, J. P.; Freed, J. H. Dynamics and Ordering in Mixed Model Membranes of Dimyristoylphosphatidylcholine and Dimyristoylphosphatidylserine: A 250 GHz Electron Spin Resonance Study Using Cholestane. *Biophys. J.* **1998**, *75*, 2532−2546.
(41) Shapiro, Y. E.; Meirovitch, E. Slowly Relaxing Local Structure (SRLS) Analysis of ^{15}N−H Relaxation from the Prototypical Small Proteins GB1 and GB3. *J. Phys. Chem. B* **2012**, *116*, 4056−4068.
(42) Fu, Y.; Kasinath, V.; Moorman, V. R.; Nucci, N. V.; Hilser, V. J.; Wand, A. J. Coupled Motion in Proteins Revealed by Pressure Perturbation. *J. Am. Chem. Soc.* **2012**, *134*, 8543−8550.
(43) Song, X.-J.; Flynn, P. F.; Sharp, K. A.; Wand, A. J. Temperature Dependence of Fast Dynamics in Proteins. *Biophys. J.* **2007**, *92*, L43−L45.
(44) Caro, J. A.; Harpole, K. W.; Kasinath, V.; Lim, J.; Granja, J.; Valentine, K. G.; Sharp, K. A.; Wand, A. J. Entropy in Molecular Recognition by Proteins. *Proc. Natl. Acad. Sci. U.S.A.* **2017**, *114*, 6563−6568.

https://dx.doi.org/10.1021/acs.jpcb.0c02662
J. Phys. Chem. B 2020, 124, 4284−4292